

Joint Super-Resolution Using Only One Anisotropic Low-Resolution Image per q-Space Coordinate

Vladimir Golkov, Jonathan I. Sperl, Marion I. Menzel, Tim Sprenger, Ek Tsoon Tan, Luca Marinelli, Christopher J. Hardy, Axel Haase, and Daniel Cremers

Abstract Recently, super-resolution methods for diffusion MRI capable of retrieving high-resolution diffusion-weighted images were proposed, yielding a resolution beyond the scanner hardware limitations. These techniques rely on acquiring either *one isotropic* or *several anisotropic* low-resolution versions of each diffusion-weighted image. In the present work, a variational formulation of joint super-resolution of all diffusion-weighted images is presented which takes advantage of interrelations between similar diffusion-weighted images. These interrelations allow to use only *one anisotropic* low-resolution version of each diffusion-weighted image and to retrieve its missing high-frequency components from other images which have a similar q-space coordinate but a different resolution-anisotropy orientation. An acquisition scheme that entails complementary resolution-anisotropy among neighboring q-space points is introduced. High-resolution images are recovered at reduced scan time requirements compared to state-of-the-art anisotropic super-resolution methods. The introduced principles of joint super-resolution thus have the potential to further improve the performance of super-resolution methods.

V. Golkov (✉) • T. Sprenger
GE Global Research, Garching, Germany

Technische Universität München, Garching, Germany
e-mail: golkov@in.tum.de; sprenger@ge.com

J.I. Sperl • M.I. Menzel
GE Global Research, Garching, Germany
e-mail: menzel@ge.com; sperl@ge.com

E.T. Tan • L. Marinelli • C.J. Hardy
GE Global Research, Niskayuna, NY, USA
e-mail: ek.tan@ge.com; marinell@research.ge.com; hardycj@ge.com

A. Haase • D. Cremers
Technische Universität München, Garching, Germany
e-mail: axel.haase@tum.de; cremers@tum.de

1 Introduction

Diffusion MRI allows measuring the molecular self-diffusion of water in biological tissue, and provides unique information on tissue microstructure unavailable to other non-invasive imaging techniques. Diffusion MRI has the potential to improve the diagnosis of, inter alia, multiple sclerosis [11], traumatic brain injury [26], and many kinds of cancer [19]. This potential stems from its ability to determine the macroscopic orientation and “bulk statistics” of diffusion within the underlying macroscopic cellular architecture. This is done by acquiring diffusion-weighted images for different diffusion directions and diffusion weightings (constituting a three-dimensional diffusion space, the q -space), and fitting a diffusion model to the measurements. For details, please refer to [12, 13].

A major challenge in diffusion MRI is balancing between acquisition duration, image resolution and signal-to-noise ratio (SNR). Numerous denoising methods were proposed to increase SNR by incorporating prior knowledge into postprocessing [15, 28] or directly into image reconstruction [10].

Another approach to improve the balance between scan time, resolution and SNR is to increase image resolution via super-resolution techniques.

1.1 *Non-diffusion MRI Super-Resolution*

Numerous super-resolution methods are available for non-diffusion MRI [20, 29]. Notably, the total generalized variation (TGV) [2, 14] regularizer, which prevents staircasing artifacts by modeling higher-order derivatives of the image, was applied to super-resolution of isotropic low-resolution MRI volumes [17].

1.2 *Diffusion MRI Super-Resolution*

In contrast to conventional diffusion MRI techniques, super-resolution methods for diffusion MRI exceed the scanner hardware limitations on image resolution.

Fiber-based methods reconstruct super-resolution information on nerve fiber bundles from conventional diffusion MRI [4–6, 18], or enhance the resolution of diffusion-weighted images by using estimated underlying nerve fiber orientations for the super-resolution model [31].

Patch-based super-resolution [8] uses *one isotropic* low-resolution version of a diffusion-weighted image, and performs super-resolution using self-similarity [3, 16, 24] of the image. In *collaborative* patch-based super-resolution [8], a high-resolution non-diffusion-weighted image is used to retrieve high-frequency information for the isotropic low-resolution diffusion-weighted image, in addition to the self-similarity prior.

The methods introduced by Scherrer et al. [25] and Poot et al. [22] use *several anisotropic* low-resolution versions of each diffusion-weighted image with complementary resolution-anisotropy orientations. Resolution anisotropy is achieved by anisotropic k-space sampling, meaning that high frequencies are not sampled for all directions equally. Subsequently, each high resolution diffusion-weighted image is reconstructed independently by using the complementary high-frequency information from the anisotropic low-resolution acquisitions. Several anisotropic low-resolution acquisitions with different distortions are used in [23] for joint susceptibility artifact correction and super-resolution.

Model-based super-resolution [27] introduces a framework to estimate high-resolution parameter maps for an arbitrary diffusion model from *several anisotropic* low-resolution versions of each diffusion-weighted image. As a proof of concept, the authors use the ball-and-stick model [1] and apply the method to an in silico phantom. Model-based super-resolution uses information from the entire q-space simultaneously, and is shown to outperform independent super-resolution of individual diffusion-weighted images. However, information on high frequencies is still completely acquired for every q-space coordinate—several acquisitions per q-space coordinate are used.

Three different combination schemes of q-space coordinates and resolution-anisotropy orientations were proposed for tomographic reconstruction of diffusion tensors [7]. However, the scheme that uses only *one anisotropic* acquisition per q-space coordinate restricts the resolution-anisotropy orientation exactly to the respective diffusion gradient direction.

We propose a super-resolution method for diffusion MRI that jointly recovers high frequencies of all diffusion-weighted images, but requires only *one anisotropic* low-resolution acquisition per q-space coordinate. The resolution-anisotropy orientations are chosen such that neighbors in q-space possess complementary high-frequency information, and regularization along q-space allows them to propagate this information to each other.

2 Methods

Two formulations for joint super-resolution of five-dimensional data (2-D image space and 3-D q-space) are introduced, relying on two respective imaging models: the formation of low-resolution images from high-resolution images, or the formation of acquired subsampled k-space raw data from underlying high-resolution images.

2.1 Image Formation Model

In the following, five-dimensional data are considered. The 5-D low-resolution images \mathbf{y} are formed from the high-resolution images $\boldsymbol{\rho}$ in the following way:

$$\mathbf{y} = \mathbf{D}\boldsymbol{\rho} + \boldsymbol{\epsilon}_{\mathbf{y}}, \quad (1)$$

where \mathbf{D} is the blur and downsampling operator [8, 27], and $\boldsymbol{\epsilon}_{\mathbf{y}}$ is the residual noise. The model for the acquired k-space data \mathbf{d} is

$$\mathbf{d} = \mathbf{U}\mathcal{F}_{x \rightarrow k}\boldsymbol{\rho} + \boldsymbol{\epsilon}_{\mathbf{d}}, \quad (2)$$

where $\mathcal{F}_{x \rightarrow k}$ is the Fourier transform from image space (x-space) to k-space along two of the five data dimensions, \mathbf{U} is the undersampling operator in k-space (omitting high frequencies in a certain orientation), and $\boldsymbol{\epsilon}_{\mathbf{d}}$ is complex-valued i.i.d. Gaussian noise.

2.2 k-q Acquisition Scheme

For the present purpose, coordinates in q-space are sampled on a regular Cartesian grid up to a maximum diffusion weighting b_{\max} , as in diffusion spectrum imaging (DSI) [30]. For each q-space point, only *one anisotropic* low-resolution image is acquired by omitting high frequencies in k-space in one direction, see Fig. 1. The resolution-anisotropy directions are chosen such that neighboring points in q-space contain complementary high-frequency information. For an image lacking vertical high frequencies, all of its six Cartesian-grid q-space neighbors contain vertical high frequencies but lack horizontal high frequencies—and vice versa. Figure 2 illustrates this relationship.

2.3 Joint Super-Resolution

We perform super-resolution for all diffusion-weighted images jointly. The data in our formulation is thus five-dimensional (2-D image space and 3-D q-space). TGV [2, 14] along all five data dimensions is applied as a regularization term. This regularization has a threefold effect:

- Regularization along q-space propagates complementary high-frequency information between q-space-neighboring diffusion-weighted images of different resolution-anisotropy orientations (Fig. 2).

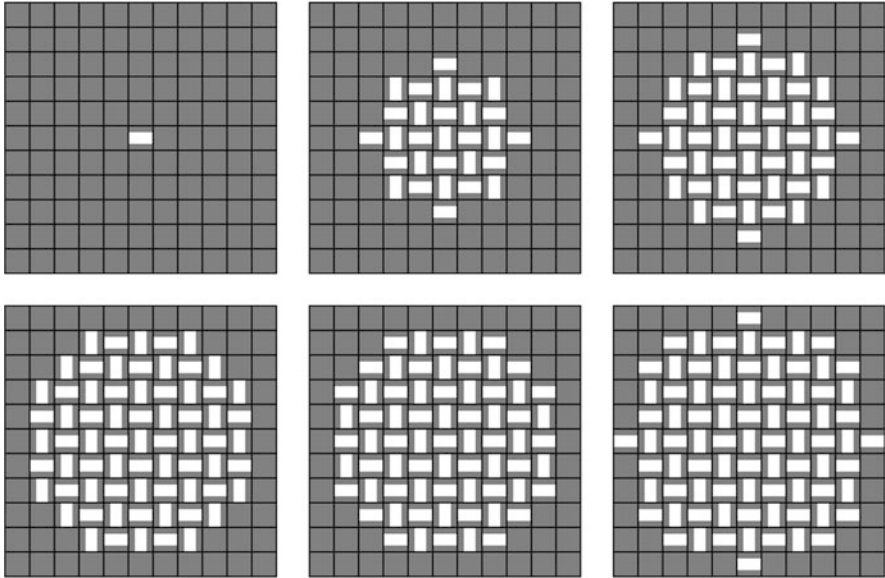


Fig. 1 Sampling scheme in joint k-q space. The *six large squares* correspond to q-space DSI coordinates $q_z = -5 \dots 0$ (coordinates $q_z = 1 \dots 5$ analogous to $q_z = -1 \dots -5$ not depicted). The *small squares within each large square* correspond to coordinates $q_x = -5 \dots 5$, $q_y = -5 \dots 5$. The *small squares* depict sampled (*white*) and unsampled (*gray*) k-space points for each q-space coordinate. Sampling anisotropy in k-space results in resolution anisotropy in image space, and the anisotropy orientations are chosen such that neighbors in q-space have complementary high-frequency information in horizontal and vertical directions (cf. Fig. 2)

- The image model of TGV introduces prior knowledge capable of retrieving missing high frequencies when regularizing along image space in a super-resolution framework [17].
- TGV regularization along five dimensions reconstructs missing information in 5-D space and reduces noise [9].

Second-order TGV is a piecewise-smooth image model, formulated [2, 14] as

$$\text{TGV}(\rho) = \min_{\mathbf{v}} \int_{\Omega} \alpha_1 |\nabla \rho - \mathbf{v}| dx + \alpha_0 \int_{\Omega} |\mathcal{E}(\mathbf{v})| dx, \quad (3)$$

where $\mathcal{E}(\mathbf{v}) = \frac{1}{2} (\nabla \mathbf{v} + \nabla \mathbf{v}^T)$ is the symmetrized derivative, α_1 and α_0 are regularization parameters, and Ω is the image domain (field of view). TGV balances the first and second derivatives of the image via the vector field \mathbf{v} , allowing both affine regions and edges.

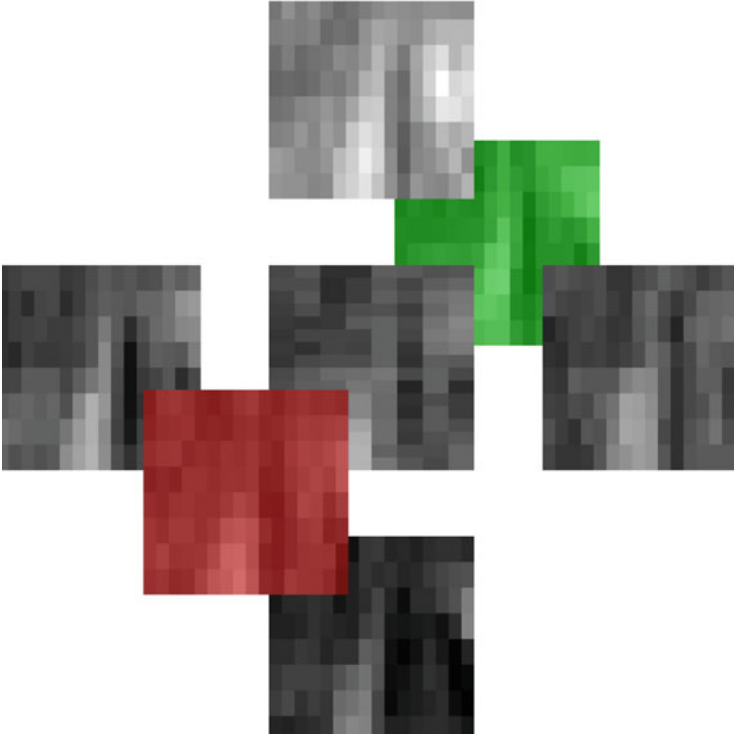


Fig. 2 Detail of a low-resolution image (*middle*) and its six neighbors in Cartesian q -space along q_x (*left, right*), along q_y (*bottom, top*) and along q_z (*red, green*). The *middle image* lacks horizontal resolution, but its six q -space neighbors all have high horizontal resolution, and the information they contain is propagated to the middle image in iterative joint super-resolution via regularization along q -space. The same principle analogously applies to images lacking vertical resolution. Middle image taken from DSI q -space coordinate $(q_x, q_y, q_z) = (0, -3, 1)$

Joint super-resolution is formulated in a variational framework. To estimate high-resolution images $\hat{\rho}$ from low-resolution images \mathbf{y} formed according to the model in Eq. (1), the following optimization problem is solved:

$$\hat{\rho} = \arg \min_{\rho} \|\mathbf{D}\rho - \mathbf{y}\|_2^2 + \text{TGV}(\rho) . \quad (4)$$

To obtain high-resolution 5-D image estimates $\hat{\rho}$ from raw k -space data \mathbf{d} formed according to the imaging model in Eq. (2), the following optimization problem is solved:

$$\hat{\rho} = \arg \min_{\rho} \|\mathbf{U}_{\mathcal{F}_x \rightarrow k}\rho - \mathbf{d}\|_2^2 + \text{TGV}(\rho) . \quad (5)$$

In both cases, solutions are obtained with a first-order primal-dual algorithm [21].

2.4 Experiments

As a proof of concept, the resolution of a healthy volunteer scan was retrospectively reduced according to the scheme described in Sect. 2.2. In this way, comparison to the original high-resolution data was possible. The scan was performed using a single coil on a 3T GE MR750 clinical MR scanner (GE Healthcare, Milwaukee, WI, USA) with the following imaging parameters: $T_R = 2535$ ms, $T_E = 93.3$ ms, 515 DSI q-space coordinates within the sphere inscribed in a $11 \times 11 \times 11$ Cartesian grid, $b_{\max} = 2000$ s/mm², voxel size $1.875 \times 1.875 \times 4$ mm. Thus, the artificially downsampled resolution was $1.875 \times 3.75 \times 4$ mm and $3.75 \times 1.875 \times 4$ mm, depending on q-space coordinate, cf. Fig. 1. Informed consent was obtained.

Joint super-resolution from low-resolution image space, Eq. (4), and from low-resolution (undersampled) k-space data, Eq. (5), was performed.

3 Results

Joint super-resolution results are shown in Fig. 3. Joint super-resolution, especially from k-space data \mathbf{d} , largely removes low-resolution artefacts which manifest themselves as underestimations and overestimations (blue and red in the bottom rows of Fig. 3) of the true signal around salient image features.

Six of the acquired 515 q-space coordinates, namely $(q_x, q_y, q_z) = (\pm 5, 0, 0)$, $(0, \pm 5, 0)$ and $(0, 0, \pm 5)$, have only one neighbor in q-space. We observed that low-resolution artefacts remained at these coordinates (not shown). Due to this issue, but also for the sake of optimization of the entire protocol, adaptive regularizers and/or further development of the sampling scheme might be beneficial for joint super-resolution.

Peak signal to noise ratio (PSNR) was calculated, which is defined as

$$\text{PSNR} = 20 \log_{10}(\text{MAX}/\text{RMSE}) , \quad (6)$$

where MAX is the maximal intensity of the image and RMSE is the root mean squared error of the image compared to the high-resolution original. PSNR was 40.69 dB for low-resolution images, which could be improved to 41.33 dB for joint super-resolution images reconstructed from low-resolution images via the optimization problem (4), and 41.37 dB for joint super-resolution from k-space data by solving (5). Since the original high-resolution image is noisy, its noise is also captured in the calculation of PSNR, preventing the distinction between noise and low-resolution artifact removal. However, artifacts are visibly removed by the joint super-resolution method, cf. Fig. 3.

Besides, the denoising effect [9] of regularization of the five-dimensional data can also be observed in our results (joint super-resolution results contain less noise than the original high-resolution images, and a great part of the incoherent noise in

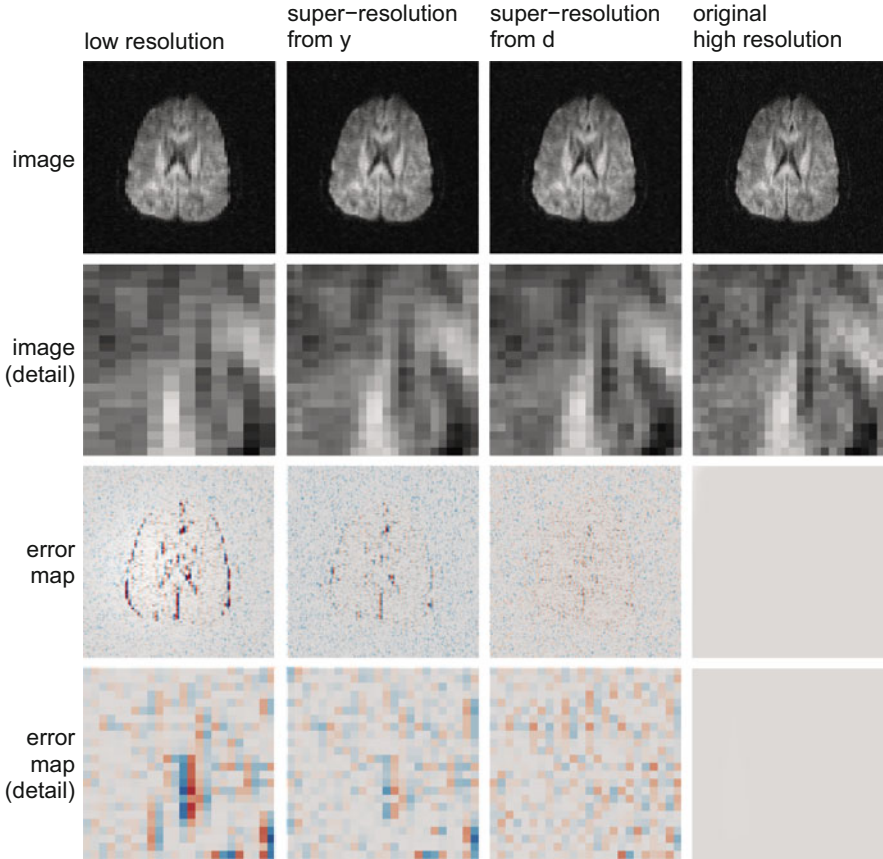


Fig. 3 Comparison of low-resolution images, high-resolution images retrieved by joint super-resolution, and original high-resolution images with full k-space coverage. Error maps compared to the high-resolution original are shown in the *third* and *fourth* row. DSI q-space coordinate $(q_x, q_y, q_z) = (0, -3, 1)$ is shown

the error maps, Fig. 3, is caused by noise in the original high-resolution image). This indicates that the improved stability to noise when using TGV for super-resolution as reported in [17] also benefits *joint* super-resolution.

4 Discussion and Conclusions

Two formulations for joint super-resolution of 5-D data were introduced along with a k-q acquisition scheme. Joint super-resolution from k-space, Eq. (5), outperformed joint super-resolution from low-resolution image space, Eq. (4), in terms of PSNR and visual image quality. This result can be attributed inter alia to an imperfect

approximation of \mathbf{D} in the image space model, cf. [8, 22, 25, 27]. Both joint super-resolution formulations were able to enhance fine details in diffusion-weighted images.

All in all, acquiring only one anisotropic image per q-space point strongly reduces the imaging time compared to state-of-the-art super-resolution techniques. We demonstrated that it is feasible to retrieve missing high-resolution information using an appropriate regularization and complementary resolution-anisotropy orientations among q-space neighbors.

With this scan time reduction in prospect, future work may focus on optimizing the protocol in terms of motion and distortion compensation [22, 25], q-space coordinates, maximal b-value, anisotropy orientations and downsampling factors in order to match a realistic clinical setting and compare the performance of joint super-resolution to state-of-the-art super-resolution methods. From the discussed results we conclude that the introduced principles of joint super-resolution have the potential to further improve the performance of super-resolution methods.

Acknowledgements Grant support: Deutsche Telekom Foundation.

References

1. Behrens, T.E.J., Woolrich, M.W., Jenkinson, M., Johansen-Berg, H., Nunes, R.G., Clare, S., Matthews, P.M., Brady, J.M., Smith, S.M.: Characterization and propagation of uncertainty in diffusion-weighted MR imaging. *Magn. Reson. Med.* **50**, 1077–1088 (2003). doi:10.1002/mrm.10609
2. Bredies, K., Kunisch, K., Pock, T.: Total generalized variation. *SIAM J. Imaging Sci.* **3**, 492–526 (2010). doi:10.1137/090769521
3. Buades, A., Coll, B., Morel, J.M.: A review of image denoising algorithms, with a new one. *Multiscale Model. Simul.* **4**, 490–530 (2005). doi:10.1137/040616024
4. Calamante, F., Tournier, J.-D., Jackson, G.D., Connelly, A.: Track-density imaging (TDI): super-resolution white matter imaging using whole-brain track-density mapping. *NeuroImage* **53**, 1233–1243 (2010). doi:10.1016/j.neuroimage.2010.07.024
5. Calamante, F., Tournier, J.-D., Heidemann, R.M., Anwander, A., Jackson, G.D., Connelly, A.: Track density imaging (TDI): validation of super resolution property. *NeuroImage* **56**, 1259–1266 (2011). doi:10.1016/j.neuroimage.2011.02.059
6. Calamante, F., Tournier, J.-D., Kurniawan, N.D., Yang, Z., Gyengesi, E., Galloway, G.J., Reutens, D.C., Connelly, A.: Super-resolution track-density imaging studies of mouse brain: comparison to histology. *NeuroImage* **59**, 286–296 (2012). doi:10.1016/j.neuroimage.2011.07.014
7. Cheryauka, A.B., Lee, J.N., Samsonov, A.A., Defrise, M., Gullberg, G.T.: MRI diffusion tensor reconstruction with PROPELLER data acquisition. *Magn. Reson. Imaging* **22**, 139–148 (2004). doi:10.1016/j.mri.2003.08.001
8. Coupé, P., Manjón, J.V., Chamberland, M., Descoteaux, M., Hiba, B.: Collaborative patch-based super-resolution for diffusion-weighted images. *NeuroImage* **83**, 245–261 (2013). doi:10.1016/j.neuroimage.2013.06.030
9. Golkov, V., Menzel, M.I., Sprenger, T., Souiai, M., Haase, A., Cremers, D., Sperl, J.I.: Direct reconstruction of the average diffusion propagator with simultaneous compressed-sensing-accelerated diffusion spectrum imaging and image denoising by means of total generalized

- variation regularization. In: Proceedings of Joint Annual Meeting ISMRM-ESMRMB, Milan, Italy, 10–16 May 2014, p. 4472
10. Haldar, J.P., Wedeen, V.J., Nezamzadeh, M., Dai, G., Weiner, M.W., Schuff, N., Liang, Z.-P.: Improved diffusion imaging through SNR-enhancing joint reconstruction. *Magn. Reson. Med.* **69**, 277–289 (2013). doi:10.1002/mrm.24229
 11. Inglese, M., Bester, M.: Diffusion imaging in multiple sclerosis: research and clinical implications. *NMR Biomed.* **23**, 865–872 (2010). doi:10.1002/nbm.1515
 12. Johansen-Berg, H., Behrens, T.E.J. (eds.): *Diffusion MRI: From Quantitative Measurement to In-vivo Neuroanatomy*, 2nd edn. Academic, New York (2013)
 13. Jones, D.K. (ed.): *Diffusion MRI: Theory, Methods and Applications*. Oxford University Press, Oxford (2010)
 14. Knoll, F., Bredies, K., Pock, T., Stollberger, R.: Second order total generalized variation (TGV) for MRI. *Magn. Reson. Med.* **65**, 480–491 (2011). doi:10.1002/mrm.22595
 15. Lam, F., Babacan, S.D., Haldar, J.P., Weiner, M.W., Schuff, N., Liang, Z.-P.: Denoising diffusion-weighted magnitude MR images using rank and edge constraints. *Magn. Reson. Med.* **71**, 1272–1284 (2014). doi:10.1002/mrm.24728
 16. Manjón, J. V, Coupé, P., Buades, A., Fonov, V., Louis Collins, D., Robles, M.: Non-local MRI upsampling. *Med. Image Anal.* **14**, 784–792 (2010). doi:10.1016/j.media.2010.05.010
 17. Martín, A., Marquina, A., Hernández-Tamames, J.A., García-Polo, P., Schiavi, E.: MRI TGV based super-resolution. In: Proceedings of the ISMRM 21st Annual Meeting, Salt Lake City, 20–26 Apr 2013, p. 2696
 18. Nedjati-Gilani, S., Alexander, D.C., Parker, G.J.M.: Regularized super-resolution for diffusion MRI. In: 5th IEEE International Symposium on Biomedical Imaging: From Nano to Macro, Paris, 14–17 May 2008, pp. 875–878
 19. Padhani, A.R., Liu, G., Mu-Koh, D., Chenevert, T.L., Thoeny, H.C., Ross, B.D., Cauteren, M. Van, Collins, D., Hammoud, D.A., Rustin, G.J.S., Taouli, B.: Diffusion-weighted magnetic resonance imaging as a cancer biomarker: consensus and recommendations. *Neoplasia* **11**, 102–125 (2009). doi:10.1593/neo.81328
 20. Plenge, E., Poot, D.H.J., Bernsen, M., Kotek, G., Houston, G., Wielopolski, P., van der Weerd, L., Niessen, W.J., Meijering, E.: Super-resolution methods in MRI: can they improve the trade-off between resolution, signal-to-noise ratio, and acquisition time? *Magn. Reson. Med.* **68**, 1983–1993 (2012). doi:10.1002/mrm.24187
 21. Pock, T., Cremers, D., Bischof, H., Chambolle, A.: An algorithm for minimizing the Mumford–Shah functional. In: 12th International Conference on Computer Vision (ICCV). pp. 1133–1140. IEEE, Kyoto (2009)
 22. Poot, D.H.J., Jeurissen, B., Bastiaensen, Y., Veraart, J., Van Hecke, W., Parizel, P.M., Sijbers, J.: Super-resolution for multislice diffusion tensor imaging. *Magn. Reson. Med.* **69**, 103–113 (2013). doi:10.1002/mrm.24233
 23. Ruthotto, L., Mohammadi, S., Weiskopf, N.: A new method for joint susceptibility artefact correction and super-resolution for dMRI. In: Proceedings of SPIE 9034, Medical Imaging 2014: Image Processing, San Diego, 15 Feb 2014
 24. Rousseau, F.: A non-local approach for image super-resolution using intermodality priors. *Med. Image Anal.* **14**, 594–605 (2010). doi:10.1016/j.media.2010.04.005
 25. Scherrer, B., Gholipour, A., Warfield, S.K.: Super-resolution anisotropic reconstruction to increase the spatial resolution of diffusion weighted images from orthogonal anisotropic acquisitions. *Med. Image Anal.* **16**, 1465–1476 (2012). doi:10.1016/j.media.2012.05.003
 26. Shenton, M.E., Hamoda, H.M., Schneiderman, J.S., Bouix, S., Pasternak, O., Rath, Y., Vu, M., Purohit, M.P., Helmer, K., Koerte, I., Lin, A.P., Westin, C.-F., Kikinis, R., Kubicki, M., Stern, R.A., Zafonte, R.: A review of magnetic resonance imaging and diffusion tensor imaging findings in mild traumatic brain injury. *Brain Imaging Behav.* **6**, 137–192 (2012). doi:10.1007/s11682-012-9156-5
 27. Tobisch, A., Neher, P.F., Rowe, M.C., Maier-Hein, K.H., Zhang, H.: Model-based super-resolution of diffusion MRI. In: Schultz, T., Nedjati-Gilani, G., Venkataraman, A., O’Donnell,

- L., Panagiotaki, E. (eds.) *Computational Diffusion MRI and Brain Connectivity, MICCAI Workshops*, pp. 25–34. Springer International Publishing, Berlin (2014)
28. Tristán-Vega, A., García-Pérez, V., Aja-Fernández, S., Westin, C.-F.: Efficient and robust nonlocal means denoising of MR data based on salient features matching. *Comput. Methods Programs Biomed.* **105**, 131–144 (2012). doi:10.1016/j.cmpb.2011.07.014
 29. Van Reeth, E., Tham, I.W.K., Tan, C.H., Poh, C.L.: Super-resolution in magnetic resonance imaging: a review. *Concepts Magn. Reson. Part A* **40**, 306–325 (2012). doi:10.1002/cmr.a.21249
 30. Wedeen, V.J., Hagmann, P., Tseng, W.-Y.I., Reese, T.G., Weisskoff, R.M.: Mapping complex tissue architecture with diffusion spectrum magnetic resonance imaging. *Magn. Reson. Med.* **54**, 1377–1386 (2005). doi:10.1002/mrm.20642
 31. Yap, P.-T., An, H., Chen, Y., Shen, D.: Fiber-driven resolution enhancement of diffusion-weighted images. *NeuroImage* **84**, 939–950 (2014). doi:10.1016/j.neuroimage.2013.09.016